

Effects of Route on Microstructural Evolution and Mechanical Properties of Cu-8 Wt Pct Ag Alloy Processed by Equal Channel Angular Pressing

YAN-ZHONG TIAN, QI-QIANG DUAN, HUA-JIE YANG, HE-FEI ZOU, GANG YANG, SHI-DING WU, and ZHE-FENG ZHANG

Equal channel angular pressing (ECAP) is applied to investigate the microstructural evolution and mechanical properties of Cu-8 wt pct Ag alloy subjected to one to four passes via four different routes (A, B_A, B_C, and C). It is demonstrated that better mechanical properties, a higher fraction of high-angle boundaries, and a smaller grain size can be obtained most rapidly with route A, whereas the specimen processed by route B_C contains relatively inhomogeneous microstructure and has poor mechanical properties. The ultimate tensile stress (UTS) of the Cu-Ag alloy processed by route B_C saturates after four passes; in contrast, the UTS of the Cu-Ag alloy processed by route A increases continuously in relation to the number of ECAP passes. Based on the experimental results, the strengthening mechanisms of the Cu-8 wt pct Ag alloy processed by different routes as well as the efficiency of different routes in refining the binary alloy are discussed.

DOI: 10.1007/s11661-010-0313-4

© The Minerals, Metals & Materials Society and ASM International 2010

I. INTRODUCTION

HIGH-STRENGTH, high-conductivity materials are significantly useful in the construction of high-field magnets.^[1] In the last 40 years, several Cu-X (Ag, Nb, Cr, and Fe) *in situ* composites, with fibrous microstructures reduced to nanoscale, have been developed by conventional cold rolling or cold drawing combined with intermediate annealing, and the strength often exceeds that estimated based on the rule of mixture.^[2-5] Of these various duplex-phase alloys, the Cu-Ag alloy has attracted considerable attention because of its superior strength and its good conductivity.^[1,6,7] It is of value to note that when the Cu-Ag alloy is cold drawn to high strains, the tensile strength can approach 2 GPa, which is significantly higher than that of the component Cu and Ag phases.^[2,7] Moreover, it generally is recognized that the high strength of such *in situ* composites is related to the decrease of the interface spacing.^[3,5,7,8] Benghalem and Morris^[7] have reported a two-stage hardening profile of Cu-Ag alloys, namely a parabolic-like hardening stage of working up to true strains of six to eight, followed by a new hardening stage at higher strain levels. The first stage is suggested to be related to work hardening, and the second stage of additional

hardening is related to the fineness of the Ag film and perhaps to its internal faulted structure.

Besides the conventional cold-working techniques, severe plastic deformation (SPD) has attracted worldwide attention in recent years because of its ability to refine substantially the coarse-grained metals or alloys down to the submicrometer or nanometer level.^[9,10] Several techniques based on SPD, such as equal channel angular pressing (ECAP),^[11-18] high-pressure torsion,^[19] dynamic plastic deformation,^[20,21] and accumulative roll bonding,^[22] have been developed widely to produce ultrafine-grained (UFG) or nanocrystalline (NC) materials. Of these various techniques, ECAP is a promising process because it can produce bulk, fully dense, and contamination-free UFG materials. Moreover, we can design and predict the microstructural evolution by using different routes (route A, B_A, B_C, and C, as defined in Reference 23).

For a Cu-Ag composite processed by conventional cold drawing or cold rolling, high strength is obtained at the sacrifice of the sample size; for example, when the original billet with 20 mm in diameter is cold drawn to a true strain of 8, the resultant material is only 0.37 mm in diameter. Fortunately, the ECAP technique may be applicable to produce such *in situ* composite with high performance and a relatively large size because high strain can be imposed without changing the cross-section area. Therefore, it is of value to note that the ECAP technique (route A) has been applied to produce such *in situ* composites.^[18,24,25] However, a more detailed investigation of the microstructural evolution and strengthening mechanism is desirable.

For the ECAP technique, it is well known that the processing route significantly affects the grain refinement and the grain shape. There are many reports on the

YAN-ZHONG TIAN, HUA-JIE YANG, and HE-FEI ZOU, Doctors, QI-QIANG DUAN, Engineer, and SHI-DING WU and ZHE-FENG ZHANG, Professors, are with the Shenyang National Laboratory for Materials Science, Institute of Metal Research, Chinese Academy of Sciences, Shenyang 110016, P.R. China. Contact e-mail: zhfzhang@imr.ac.cn GANG YANG, Professor, is with the Central Iron and Steel Research Institute, Beijing 100081, P.R. China.

Manuscript submitted October 2, 2009.

Article published online May 26, 2010

efficiency of the processing route for various materials.^[26–32] For example, either route B_C, route A, or route C has been reported to be the most effective route by different researchers. However, based on several different techniques (texture analysis and modeling), some researchers have proposed that the contradiction of the ECAP efficiency can be attributed to the difference in the intersecting angle of the die (*i.e.*, the inner angle).^[26,33] In contrast, Beyerlein *et al.*^[34] have summarized the possible reasons that may result in the contradictory reports on the efficiency of ECAP routes.

In terms of the predicted distortions of the cubic element,^[23] a fibrous structure can be obtained most rapidly with route A, which is in accordance with the morphologies made by cold drawing or cold rolling, so route A may be of great use in preparing such duplex-phase alloys. However, for the other three routes, especially routes B_C and C, the cubic element can be restored every $4n$ and $2n$ passes, respectively (n is an integer); as a result, the eutectic phases cannot be elongated into fibers. Based on the uncertainty of the efficiency of the processing route and the predicted distortion of the cubic element, it is important to study the dependence of the microstructure and the mechanical properties on the processing route.

In the current study, all four different ECAP routes are employed to conduct the Cu-8 wt pct Ag alloy up to four passes in a 90 deg die, and various techniques are used to investigate the microstructural evolution and mechanical properties. Through the ECAP technique, we expect to produce stronger Cu-X alloys before conventional cold working and to evaluate the efficiency of the ECAP route for such *in situ* composite. Because the morphology of the eutectic component varies significantly during different routes, the strengthening mechanisms induced by different routes are discussed further.

II. EXPERIMENTAL PROCEDURES

The Cu-8 wt pct Ag alloy was cast and then hot forged to 30 mm in diameter at 723 K (450 °C) to ameliorate the mechanical properties. Before pressing, the rod was annealed at 723 K (450 °C) for 10 hours to release the internal stress to facilitate the ECAP processing. After that, some billets 8 mm in diameter and 45 mm in length were cut along the rod axis. These billets were processed by ECAP at room temperature using a solid die fabricated from tool steel with two channels intersecting at an inner angle of $\Phi = 90$ deg and an outer angle of $\Psi = 30$ deg. It is known from an earlier analysis that Φ and Ψ give an imposed strain of about 1 on each pass through the die.^[35] Generally, three orthogonal directions (planes) were defined as before.^[36] All billets coated with a MoS₂ lubricant were pressed at room temperature with a pressing speed of ~ 9 mm/min⁻¹. The Cu-8 wt pct Ag alloy was subjected to one to four passes via four different routes (A, B_A, B_C, and C).^[23] After each pass of ECAP processing, the billet has to be machined; as a result, the billet is only about 25 mm in length after four passes, so the billet was not conducted further, as it would have become too

short to conduct the tensile test. Billets processed to different passes with different routes can be written in a simplified form (*e.g.*, A4 represents a sample pressed to four passes by route A, whereas A0, B_A0, C0, and B_C0 represent the as-received sample).

Before ECAP, the microstructures on the transverse section and the longitudinal section of the specimen were observed. Then, the samples processed by ECAP at each condition were characterized by scanning electron microscope (SEM). To compare the microstructural difference of the specimens deformed by the four routes, some thin slices were cut from the Y plane of the billets pressed up to four passes, and then they were examined by the LEO SUPRA35 SEM (Zeiss, Oberkochen, Germany), which was equipped with an electron back-scattering diffraction (EBSD) system. Because Cu-Ag alloys contain nearly pure Ag and Cu phases, the difference in the electropolishing rate makes the sample preparation difficult. To obtain a flatter surface and, thus, to enable area measurement of orientations for EBSD mapping, an ion milling method was developed.^[37] In this study, the EBSD technique was taken to investigate the microstructure, as it can deal with a large area and provide numerous quantitative data on the orientation distribution of both the grains and sub-grains, which is time consuming and difficult to obtain by using transmission electron microscope. A step size 50 nm was taken to construct the grain distribution and to get the quantitative information of misorientation.

The tensile specimens with gauge dimensions of $8 \times 2 \times 1$ mm and a total length of 20 mm were machined by the spark-cutting technique. Before the tensile test, all specimens were ground and polished carefully. The tensile tests were performed using an Instron 8871 testing machine at a strain rate of $\sim 5 \times 10^{-4}$ s⁻¹ at room temperature in air. Three tensile specimens of each state were tested.

III. RESULTS

The Cu-Ag binary phase diagram is shown in Figure 1,^[38] and the composition of the Cu-8 wt pct Ag alloy is indicated by the broken line. The critical Ag content for the appearance of the eutectic component is 7.9 wt pct under equilibrium condition; however, the eutectic will appear even if the Ag content is

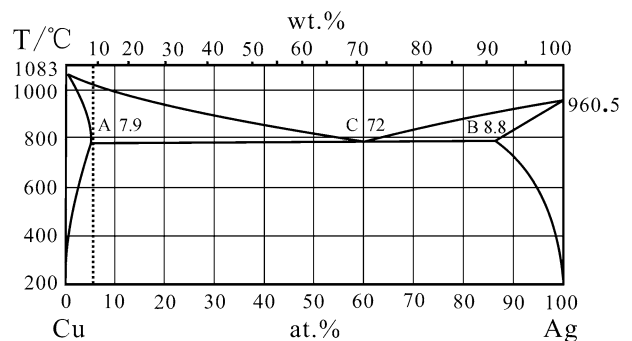


Fig. 1—Cu-Ag binary phase diagram.^[38]

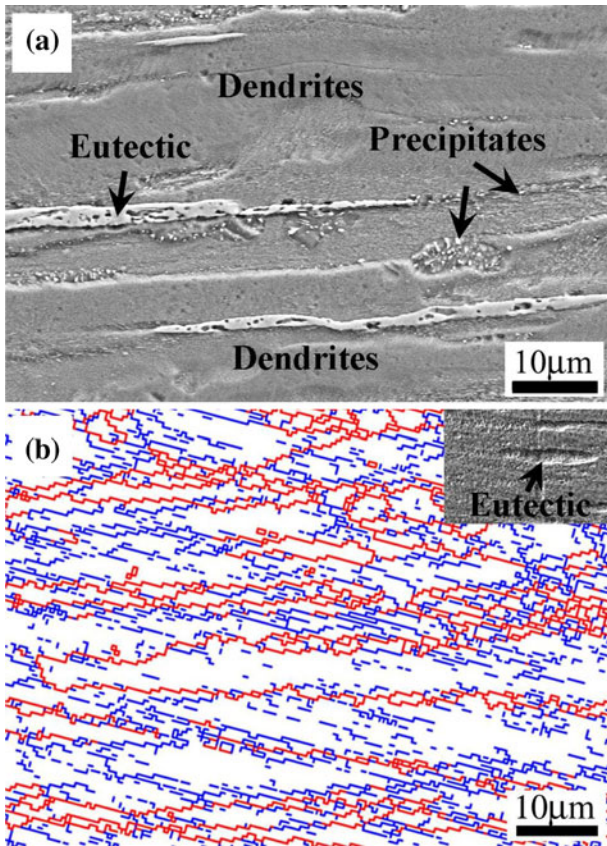


Fig. 2—Micrographs on the longitudinal section of the as-received Cu-8 wt pct Ag alloy taken by the following: (a) SEM (secondary electron micrographs); (b) EBSD (the inset shows the corresponding SEM images, and HABs and LABs are marked by red and blue lines, respectively). The horizontal direction is corresponding to the axial direction of the billets.

only 6 wt pct or 7.5 wt pct during nonequilibrium cooling.^[7,39] The effect of composition was not discussed because only one composition was adopted in this manuscript; however, the readers can refer to the previous studies.^[6,40,41] Before ECAP, the microstructure of the annealed Cu-8 wt pct Ag alloy generally is introduced first because the detailed microstructure in the as-cast, as-forged, and annealed conditions can be found elsewhere.^[39] The alloy generally contains two components—the eutectic component comprising Cu and Ag phases and the proeutectic Cu dendrite embedded with Ag precipitates (Figure 2(a)). The Ag content is 7.9 wt pct in the Cu dendrite at the eutectic temperature, which will be reduced to near zero at room temperature rapidly, leading to the formation of Ag-rich precipitates. Actually, the volume fraction of the precipitates depends on the heat treatment. The Cu and Ag phases always have the cube-on-cube orientation in the proeutectic component, but they have the orientation relationship only in selective eutectic areas.^[41] In addition, the dendrite and the eutectic component also may have the orientation relationship.^[37,42] Under the as-received condition, the eutectic region is in the micron/submicron range, whereas the precipitates are 50 nm to 90 nm in diameter.^[37] Figure 2(a) shows that

the elongated eutectic runs parallel to the axial direction of the rod, and some particle-like and rod-like Ag-rich precipitates exist near the grain boundaries. Figure 2(b) presents the EBSD map of the longitudinal plane of the rod; some banded grains, with many low-angle boundaries (LABs, $5 \leq \Delta\theta < 15$ deg) inside them, are along the axial direction. The red and blue lines represent the high-angle boundaries (HABs, $\Delta\theta \geq 15$ deg) and LABs, respectively.

A. Tensile Properties after Different ECAP Routes

Under the initial condition, the material has a yield strength of 315 MPa and a uniform elongation of ~10 pct. This is because the annealing temperature is only 450 °C, and the as-received alloy is in a work-hardened state, with numerous LABs existing in the banded grain, as shown in Figure 2(b).

Figures 3(a) through (d) show the tensile stress–strain curves of the specimens subjected to one to four ECAP passes by different routes. The mechanical properties, including yield stress (YS), ultimate tensile stress (UTS), uniform elongation, and static toughness, as a function of ECAP routes and processing passes are summarized in Table I and are elucidated in Figure 4. Figure 4(a) shows the UTS/YS as a function of the processing routes and the number of passes. It is clear that the effect of the ECAP route on the UTS/YS before three passes is gentle but gets significantly stronger as pressing up to four passes. Specimen A4 obtains the highest UTS/YS, whereas specimens C4 and B_C4 show the lowest values. The increase in UTS/YS between consecutive passes by different routes is presented in Figure 4(b); like many kinds of metals and alloys, the strength increases sharply in the first pass.^[16,17,43] After two passes, the increment in strength maintains a constant of about 60 MPa with increasing the ECAP pass by route A; for routes B_A and C, their increasing values decrease with the pressing pass, but for route B_C, its increasing value decreases continuously until about zero.

In contrast to the tensile strength, the total elongation to failure keeps nearly constant from about 10 pct to 13 pct. Moreover, the uniform elongation, which is a useful parameter for industrial application, is exhibited in Figure 4(c). Along with the enhancement in strength by route A, the uniform elongation improves slightly from 1.6 pct to 2 pct with pressing passes. In contrast, the uniform elongations of the specimens by routes B_A, C, and B_C are nearly constant at 1.6 pct \pm 0.1 pct.

UFG and NC materials have obtained a remarkable enhancement in strength; however, the elongation decreases drastically (*i.e.*, they are mutually exclusive in many cases).^[43,44] Fortunately, research on advanced materials, tailored to achieve an optimum combination of high strength and high elongation, has been performed via various methods.^[43–46] These materials should have a higher toughness in contrast to the counterparts with high strength and low elongation. Actually, few engineering materials are limited by their strength; rather they are limited by their resistance to fracture or fracture toughness.^[47] Generally, fracture toughness conventionally has been used to quantify the resistance to crack

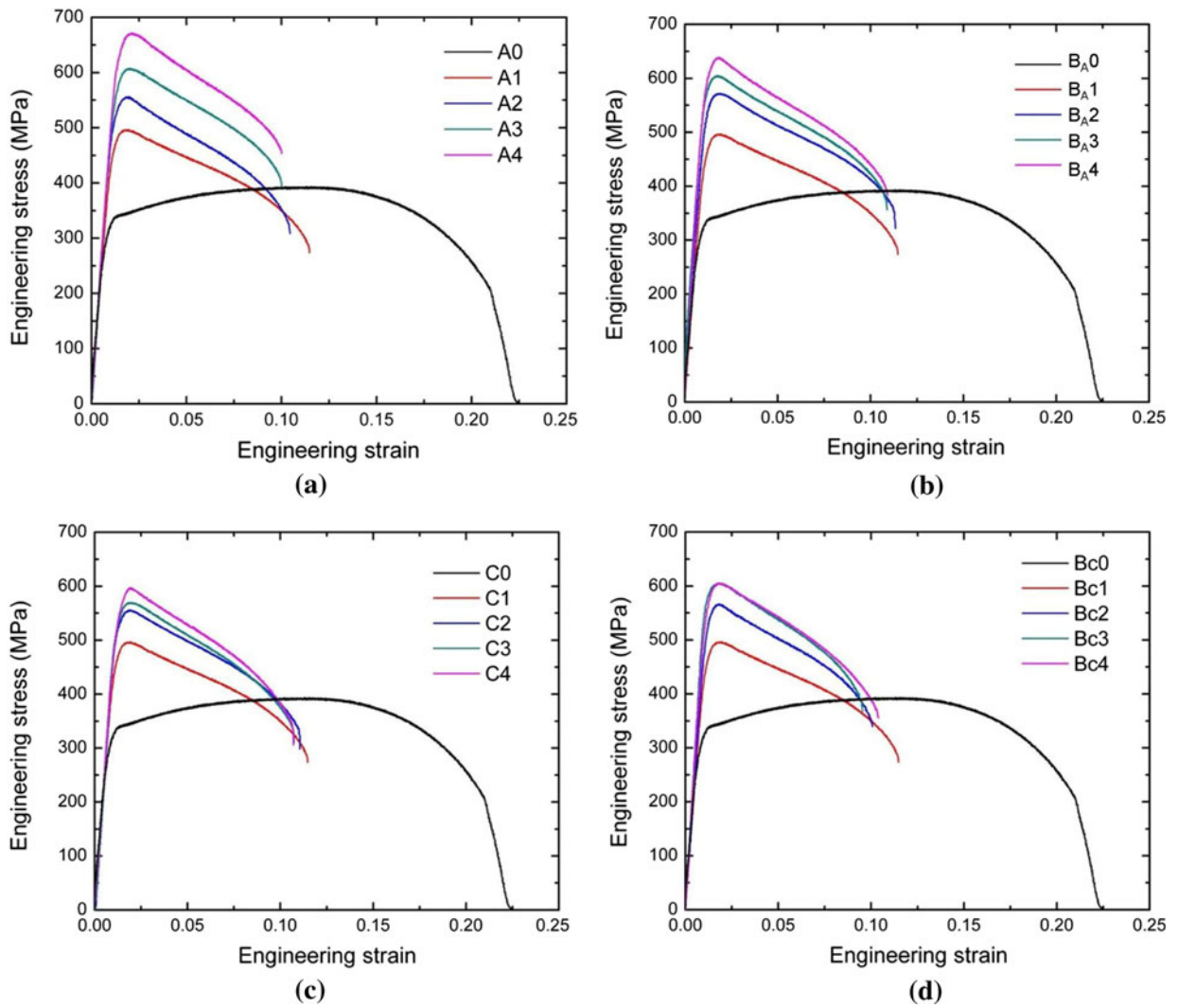


Fig. 3—Tensile engineering stress–strain curves of Cu-8 wt pct Ag alloy before and after ECAP by (a) route A, (b) route B_A, (c) route C, and (d) route B_C. The number means the ECAP passes—0 is the as-received condition; 1 is after one pass; 2 is after two passes; 3 is after three passes; 4 is after four passes.

Table I. Mechanical Properties of Cu-8 Wt Pct Ag Alloy Before and After ECAP

	ECAP Passes	0	1	2	3	4
UTS (MPa)	Route A	391	497	553	608	666
	Route B _A	391	497	570	602	636
	Route C	391	497	556	562	589
	Route B _C	391	497	565	598	589
YS (0.2 pct) (MPa)	Route A	315	461	518	574	633
	Route B _A	315	461	519	563	586
	Route C	315	461	522	536	564
	Route B _C	315	461	534	575	567
Uniform elongation (pct)	Route A	10.11	1.61	1.72	1.72	1.94
	Route B _A	10.11	1.61	1.60	1.60	1.65
	Route C	10.11	1.61	1.72	1.60	1.58
	Route B _C	10.11	1.61	1.54	1.52	1.54
Static toughness before necking (J/m ³)	Route A	—	6.15	7.44	7.57	9.56
	Route B _A	—	6.15	7.16	7.69	7.88
	Route C	—	6.15	7.31	7.04	6.53
	Route B _C	—	6.15	6.42	7.07	6.88

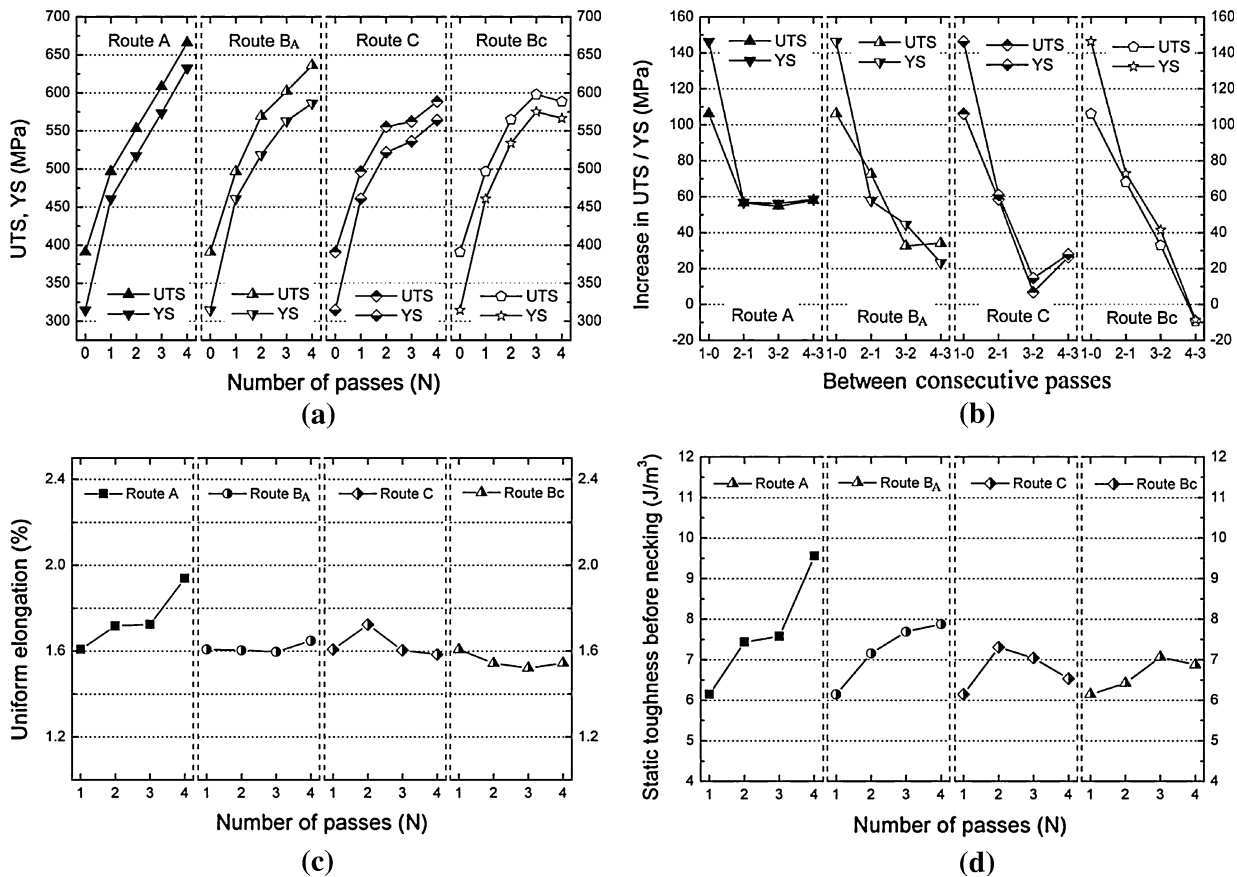


Fig. 4—Mechanical properties of Cu-8 wt pct Ag alloy before and after ECAP by different routes including (a) UTS and YS, (b) increment in UTS/YS between consecutive passes, (c) uniform elongation, and (d) static toughness before necking.

propagation. In the present study, because of the limitation of the specimen size for fracture toughness testing, another parameter comprising strength and elongation is used correspondingly to represent qualitatively the static toughness. In general, the static toughness U of materials can be calculated as follows^[48]:

$$U = \int_0^{\epsilon_f} \sigma d\epsilon \quad [1]$$

where σ is the flow stress and ϵ_f is the total strain at fracture. In other words, the static toughness U represents all plastic work absorbed by the unit volume of the tensile samples during the whole plastic deformation process up to fracture. Moreover, it is of value to note that a tensile stress–strain curve generally comprises two parts (*i.e.*, one part before necking and the other part after necking). In this study, the static toughness after necking was excluded because it was obtained after the plastic instability of materials. The static toughness before necking as a function of the number of ECAP passes and routes is exhibited in Figure 4(d). After processing by route A, the static toughness increases continuously as the pressing passes. However, the increment in the static toughness of the specimens pressed by the other three routes is not significant, to some extent, and decreases slightly for the specimens processed by route C.

To evaluate the comprehensive properties of the specimens, both the uniform elongation and the UTS are exhibited, as shown in Figure 5(a). It is clear that both the uniform elongation and the UTS upgrade to a relatively higher level by route A in contrast to the other three routes. With the increase of the ECAP pass, the samples processed by route A display a simultaneously increasing trend of the UTS and the uniform elongation, whereas the other three kinds of samples do not exhibit such a feature. Moreover, route A shows a significant improvement in UTS and static toughness than the other three routes, as shown in Figure 5(b). So it is concluded that route A is relatively more effective in improving the comprehensive mechanical properties than the other three routes for the Cu-8 wt pct Ag alloy.

For pure Cu processed by ECAP, the UTS will achieve saturation after four passes and will decrease a little after eight passes, as shown in Figure 6.^[17] It is obvious that the mechanical properties of the Cu-Ag alloy in the present study are different, which will be discussed in the subsequent section.

B. Microstructural Evolution after Different ECAP Routes

The three-dimensional (3-D) microstructures of the as-received and the as-pressed Cu-8 wt pct Ag alloy are

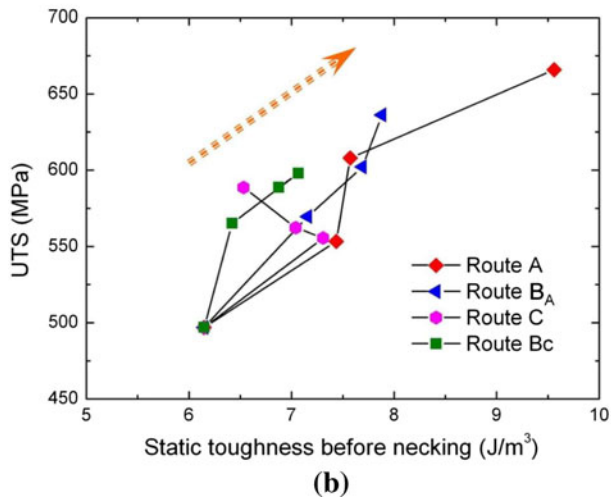
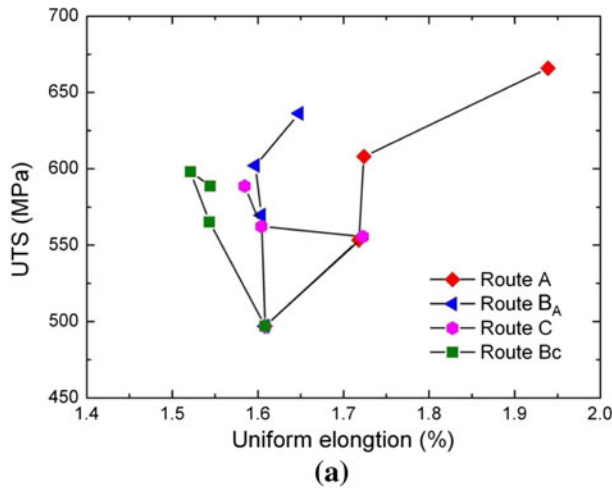


Fig. 5—Comprehensive mechanical properties of Cu-8 wt pct Ag alloy processed by the following different routes: (a) UTS and uniform elongation and (b) UTS and static toughness.

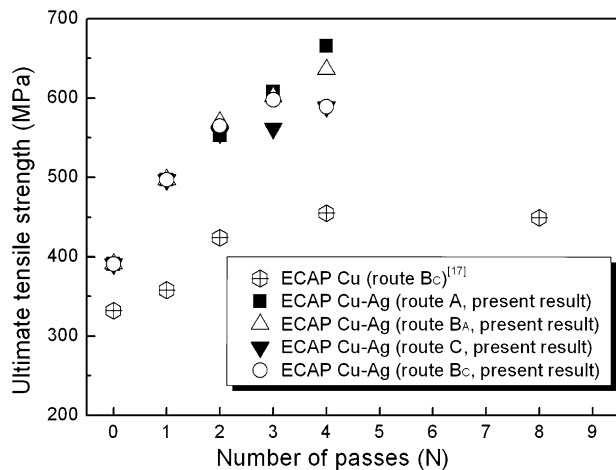


Fig. 6—Comparison of the UTS of pure Cu and Cu-Ag alloy processed by ECAP.

displayed in Figures 7(a) and (b), respectively. After one pass of ECAP, the eutectic component on the Y plane is curved in some regions as a result of imposed shear

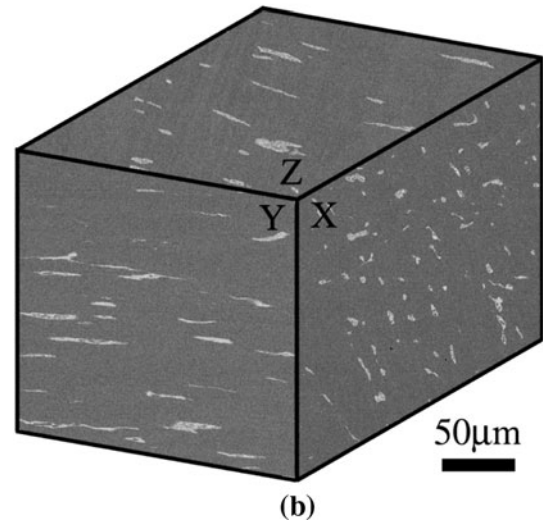
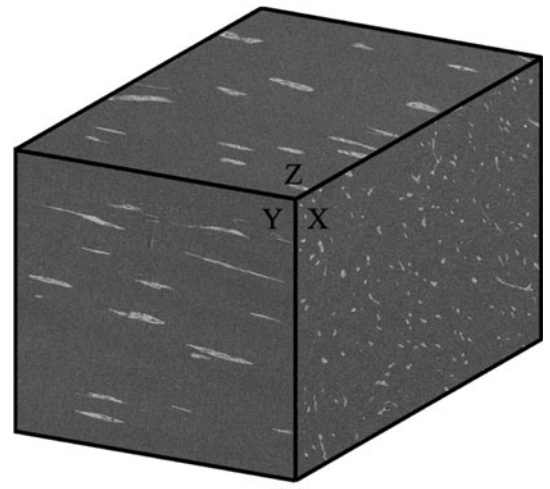


Fig. 7—Secondary electron micrographs of the (a) as-received specimen and (b) the specimen after one-pass ECAP.

strain; in contrast, the eutectic component of the as-received alloy is relatively straight. Moreover, the area of each eutectic region is about 1.5 times larger than that under the as-received condition on the X plane.

Figure 8 shows the microstructural evolution of the specimens subjected to two to four passes by different routes. It is clear that the morphologies of the eutectic component exhibit a great difference after processing by these routes. For the billets processed by route A, the eutectic regions gradually evolve into fibrous microstructures on the flow plane (Y plane). For the billets processed by route B_A, the evolution into a fibrous microstructure of the eutectic regions is slightly slower on the Y plane, but no evidence of fibrous eutectic is found on the Z plane, which is contrast with that predicted by the distortions of the cubic elements.^[23] This may be related to the initial unequipped morphology of the eutectic component. In contrast to routes A and B_A, no fibrous structure is detected on the Y plane for routes B_C and C, which is consistent with that predicted by the distortions of the cubic elements.^[23]

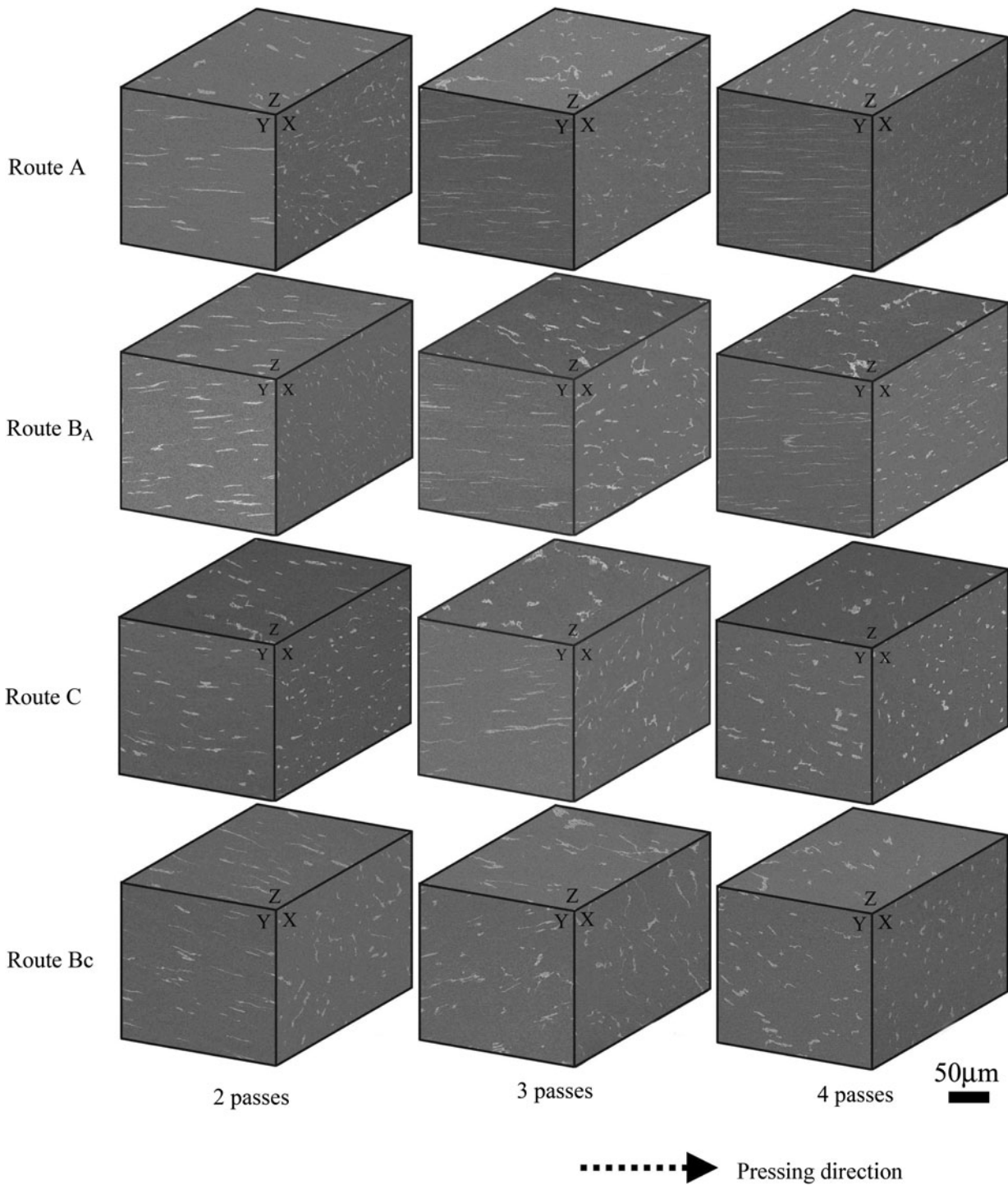


Fig. 8—Secondary electron micrographs of the specimens subjected to 2 to 4 passes by the four different ECAP routes.

Along with the microstructural evolution of the samples processed by different routes, the eutectic spacing on the Y plane is shown in Figure 9. For routes A and B_A, the eutectic spacing decreases continuously in relation to the pressing passes, whereas routes B_C and C still can retain big eutectic spacing even after four passes of ECAP.

In accord with the difference of mechanical properties when changing the pressing routes, the microstructural evolution is also different in relating to the eutectic

morphologies. Especially for those specimens processed for four passes, their mechanical properties are more sensitive to the processing routes, so the corresponding microstructure on the Y plane was investigated and is shown in Figure 10. It is found that specimens A4 and B_A4 contain a banded eutectic component, as shown in Figures 10(a) and (b). In contrast, specimens C4 and B_C4 contain relatively equiaxed eutectic, as shown in Figures 10(c) and (d). However, the investigation on this

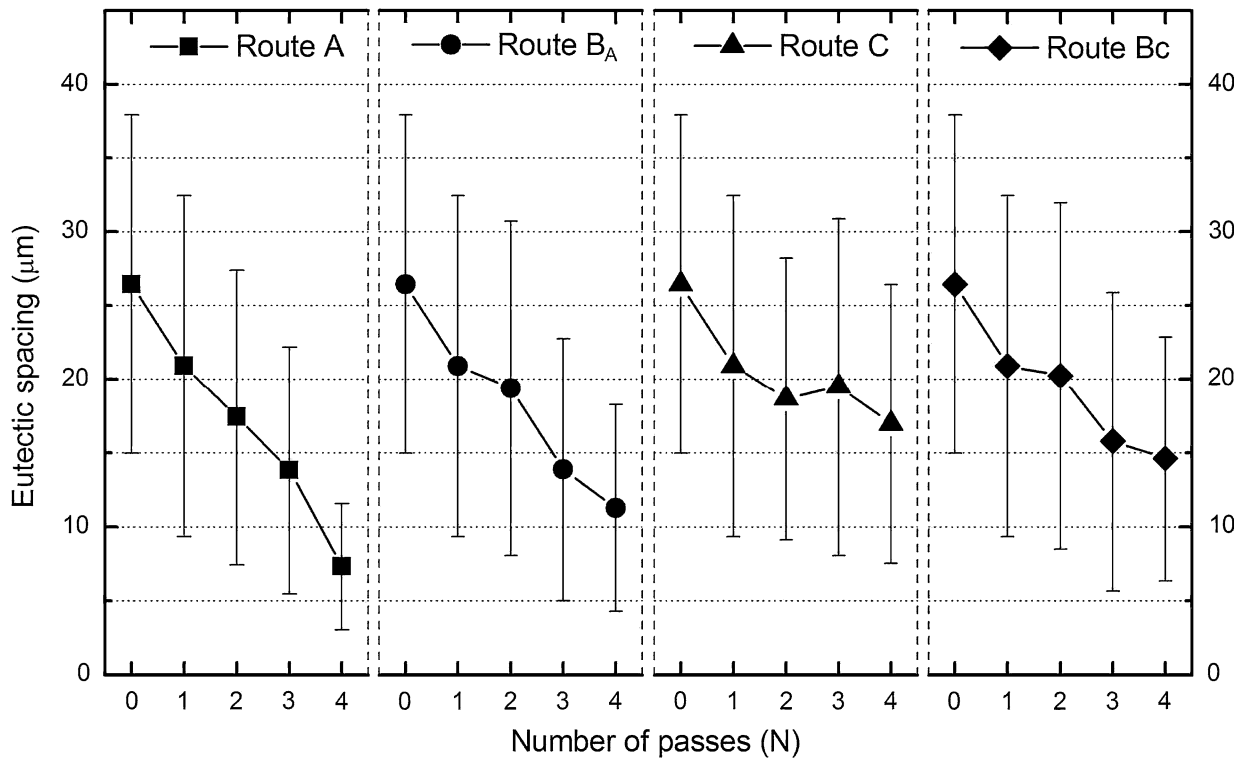


Fig. 9—Variation of the eutectic spacing on the Y plane in relation to the number of ECAP passes.

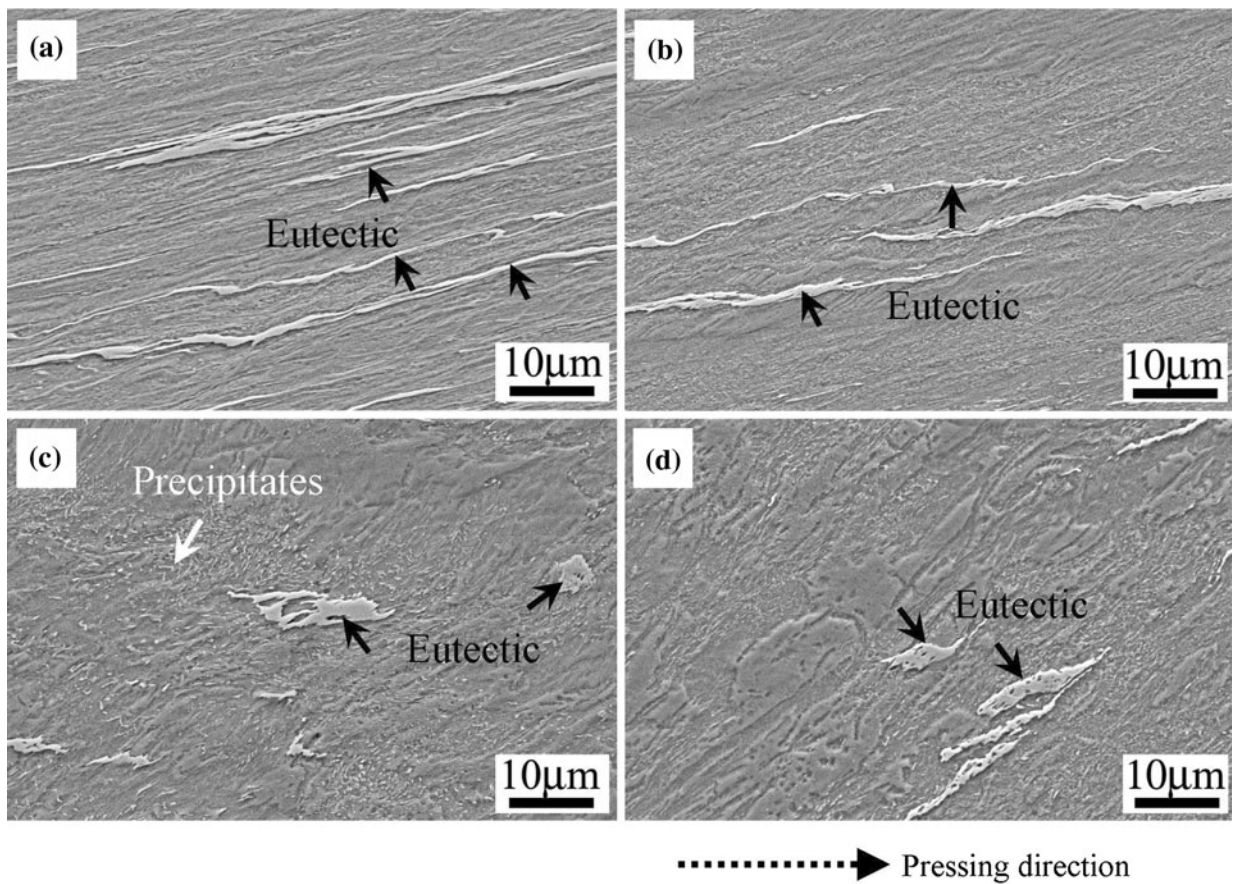


Fig. 10—Secondary electron micrographs of specimens (a) A4, (b) B_A4, (c) C4, and (d) B_c4.

microstructure is not enough; one needs to perform a more in-depth study of the grain or subgrain evolution, so the EBSD technique is employed further to investigate the microstructural differences in the specimens A4, B_A4, B_C4, and C4.

C. EBSD Analysis on Deformation Microstructures

Figures 11(a) through (d) show the EBSD results of specimens A4, B_A4, C4, and B_C4, respectively, and the inset SEM images are corresponding to the EBSD images, with the eutectic component marked by arrows. HABs and LABs are indicated by red and blue lines, respectively. From Figure 11, it is clear that there are significant differences in the deformed microstructures, which are highlighted subsequently.

For specimen A4, it is shown that the deformed microstructure is relatively uniform, and nearly no coarse grain can be detected. Generally, the region consists of elongated grains; besides, some equiaxed grains also exist. For specimen B_A4, as shown in Figure 11(b), the deformed microstructure largely consists of elongated grains. It is clear that a large banded structure with a band width of $\sim 5 \mu\text{m}$ still exists after

four passes, which is comparable with the original band width of the as-received sample. For specimen C4, large grains, several microns in diameter, exist in large areas (Figure 11(c)). Therefore, the coarse deformed microstructure of specimen C4 should be corresponding to the relatively poor mechanical property, as shown in Figure 3. For the specimen B_C4, it is of interest to note that the deformed microstructure is not uniform (Figure 11(d)). Conversely, the microstructure consists of fine grains that concentrate in bands and coarse grains that exist widely between the bands. The erratic result is contradictory with the previous reports, which always deem that route B_C is most effective in introducing HABs.^[27,28] However, there are exceptions as to the efficiency of the processing routes.^[12,29–32]

In Figure 11, it is shown that the eutectic always contains a more refined microstructure because the component Cu and Ag phases may have the same or a different orientation in the original state.^[41] Besides, it seems that the deformed microstructure does not show much dependence on the eutectic, which is different from that of the alloys containing undeformable particles.^[49] This can be from the good deformation compatibility between the eutectic and the matrix.^[37,42]

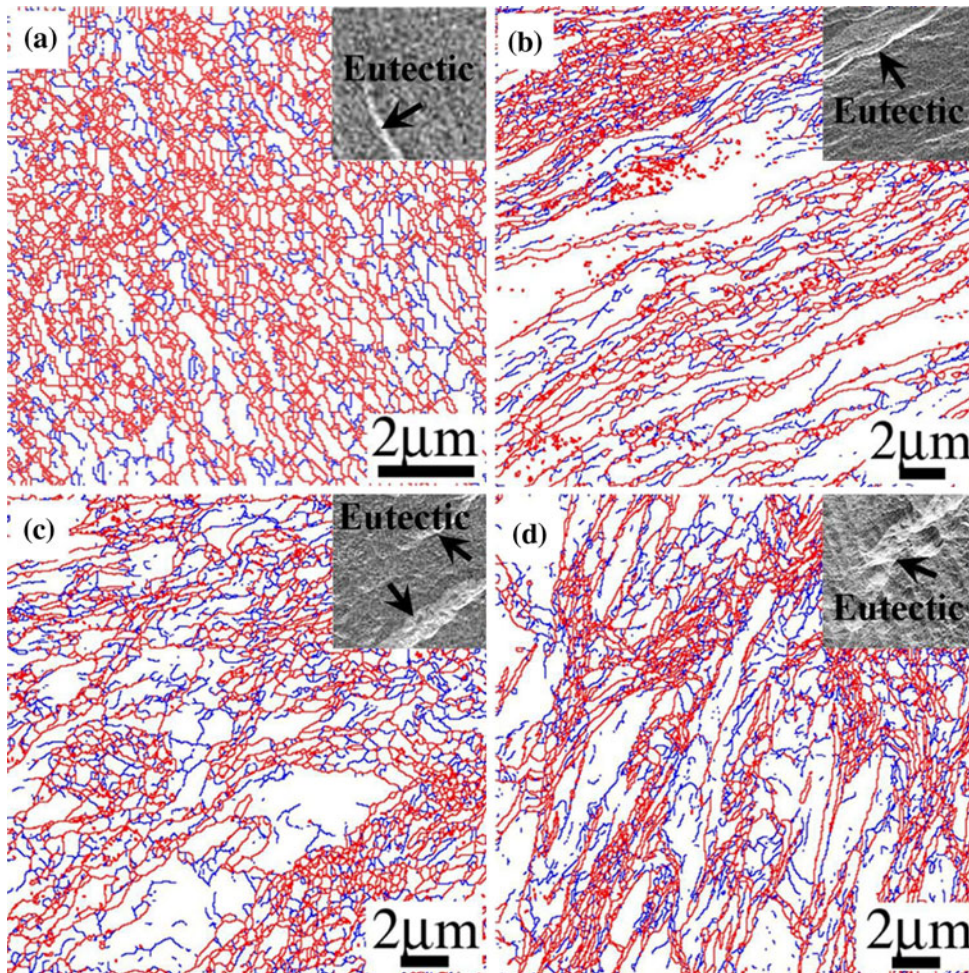


Fig. 11—EBSD maps of specimens (a) A4, (b) B_A4, (c) C4, and (d) B_C4. The eutectic component in the inset is indicated by arrows, and HABs and LABs are marked by red and blue lines, respectively. The step size is 50 nm.

The information on HABs and grain sizes is shown in Figure 12. The fraction of HABs is obtained from the orientation distribution, as shown in Figure 13, whereas the grain size is acquired from the mapping

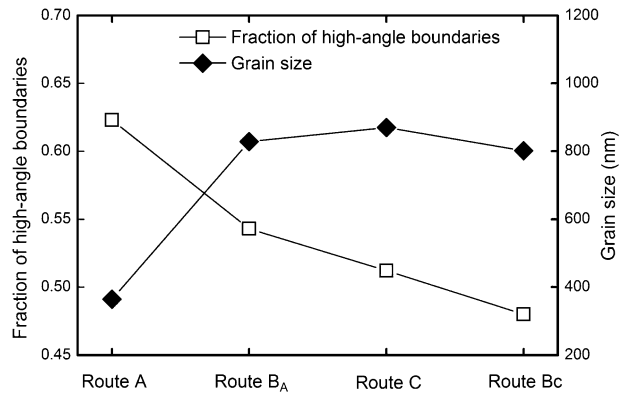


Fig. 12—Illustration of the fraction of HABs and the grain size of the specimens processed for four passes via different routes.

information in Figure 11. It is of interest to note that a larger fraction of HABs and a smaller grain size have been achieved using route A. In contrast, the fraction of HABs is lower, and the distribution of grains is rather inhomogeneous when using the other three routes. The present results are similar to those reported by Gholinia *et al.*,^[30] though the geometry of the ECAP die is different. They have demonstrated that the most effective method for forming submicron grains by ECAP is to maintain a constant strain path (route A). However, most researchers have noted that route B_C is the most effective for refining materials.^[27,28] Therefore, the issues in determining an optimized route will be discussed in the subsequent section.

IV. DISCUSSION

From the results delineated, it is obvious that the Cu-Ag alloy is sensitive to ECAP routes, and the resulting microstructure and mechanical behaviors are

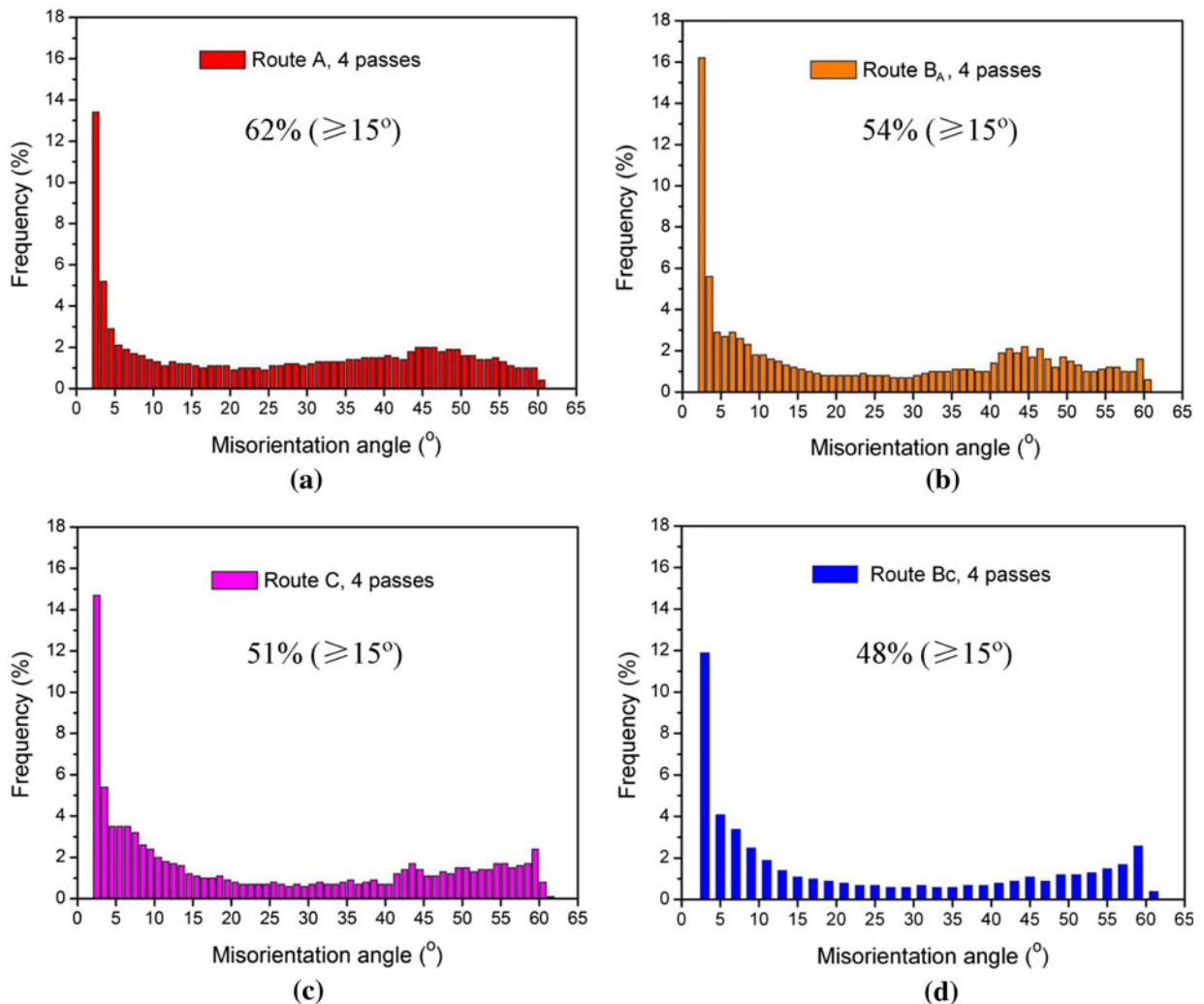


Fig. 13—Misorientation angle distribution of specimens (a) A4, (b) BA4, (c) C4, and (d) BC4.

investigated in detail. On the one hand, it is recognized that a relatively uniform microstructure can be obtained using route A, which is consistent with some results reported before^[29,30]; however, many contradictive results and conclusions are drawn by other researchers.^[27,28,31,32] Therefore, different theories and results should be analyzed, and issues on the route efficiency should be considered collectively. On the other hand, it is known that an *in situ* Cu-Ag microscale composite can be obtained using conventional cold drawing or cold rolling, and high strength has been reported, which was much higher than that of pure Cu or Ag.^[2] Therefore the strengthening mechanism of the Cu-8 wt pct Ag alloy after processing by ECAP is analyzed and discussed in the current study.

A. Efficiency of Processing Routes

Generally, either route A or route B_C is considered to be most effective in making UFG materials.^[27–30] In the previous analysis, accumulative strain and the intersection of the shear planes between consecutive passes were used to explain the effectiveness of the processing routes of ECAP.^[27–30] Iwahashi *et al.*^[32] processed high-purity Al by ECAP using a die with an inner angle of 90 deg. They suggested that route B_C is most effective and that route A is least effective in grain refinement, and they considered that the high efficiency of route B_C is a result of the 120 deg shear direction between consecutive passes. Later on, Furukawa *et al.*^[50] concluded that the development of a uniform microstructure of equiaxed grains, separated by HABs, is favored using route B_C because (1) shearing occurs across large angular ranges on the three orthogonal planes within the sample; (2) there is a regular and periodic restoration of an equiaxed microstructure during consecutive pressings; and (3) deformation occurs on each orthogonal plane. However, the fundamental grain refinement mechanism is still unclear.

In contrast to route B_C, route A also is considered to be most effective by many researchers. Prangnell *et al.*^[29] and Gholinia *et al.*^[30] conducted Al-Mg and Al-Mn alloys in a 120-deg-angle ECAP die; with the help of EBSD technique, they reported that the most effective method to form a UFG material is route A, and they also proposed a redundant strain theory to explain the results. In addition, a similar conclusion can be drawn by modeling.^[34] Based on a visco-plastic self-consistent scheme, Beyerlein *et al.*^[34] considered a 90-deg-angle ECAP die and simulated ECAP processes up to four passes for the four processing routes for an face-centered cubic (FCC) polycrystalline material. Using a grain subdivision criterion based on grain shape, they reported that route A was most effective, then route B_A and route B_C, and last route C.

Neither theory can be used commonly to explain all cases on the efficiency of ECAP routes. Fortunately, Zhu and Lowe^[26] have proposed a theory to explain the efficiency of the ECAP routes (*i.e.*, either route B_C for $\Phi = 90$ deg or route A for $\Phi = 120$ deg is most effective in refining materials). They have proposed that the interaction of shear plane with texture and crystal

structure plays a primary role in grain refinement, whereas the accumulative strain plays a secondary role. They also elucidated that the evaluation of the effectiveness of grain refinement is how close the angle between the texture plane and the shear plane is to 70.5 deg—the angle between two {111} tetrahedron planes of the FCC material. Similarly, Li^[33] had simulated the efficiency of grain refinement in ECAP based on crystal plasticity, and the optimum route for grain refinement was identified as the one with a higher number of newly activated slip systems (*i.e.*, route B for $\Phi = 90$ deg and route A for $\Phi = 120$ deg). However, Beyerlein *et al.*^[34] have predicted that none of the routes satisfied the criterion proposed by Zhu and Lowe^[26] Moreover, many articles revealed that even for $\Phi = 90$ deg, route A is still the most effective route for grain refinement,^[51,52] which is consistent with the present results of Cu-8 wt pct Ag alloy.

It is clear that the effect of processing routes on the grain refinement is still not understood fully; there are even some misleading results or conclusions. Beyerlein *et al.*^[34] have summarized the possible reasons that may result in the contradictive reports on the efficiency of ECAP routes. In our investigation, EBSD results indicate that a high microstructural heterogeneity exists after four passes, especially for those specimens processed by routes B_C, C, and B_A (Figure 11). In terms of our present results, it is expected that a continuous inclination of the grains occurs in the same plane as the number of processing passes increases for route A. As a result, the high fraction of HABs not only should originate from the grain subdivision process but also originate from the geometric changes of the grain shape.^[30,52,53] In contrast, routes B_C and C can retain their original grain shape after $4n$ and $2n$ passes, respectively, so the geometric contributions of the original grain boundaries should be much less than the newly created HABs. It also is reported that profuse shear bands introduce additional HABs in samples processed by route A.^[52] In accordance with the report, profuse shear bands also are found in the present Cu-8 wt pct Ag alloy, and they can be identified easily in such a duplex-phase alloy, as shown in Figure 14. For specimen A1, the eutectic component is staggered by shear bands, leaving deformation-induced shear traces inclined to the extrusion direction, whereas Figure 14(b) shows the serrated precipitates with every staggered region crossed by a shear band, which can be identified as faint inclined lines. Note that the space between the shear bands can be smaller than 1 μm . For specimen A4, as shown in Figures 14(c) and (d), both the eutectic and the precipitates are elongated into fibrous structure with shear bands inclined to the extrusion direction. So shear banding development also should play an important role in introducing HABs.^[54]

B. Strengthening Mechanism

1. Conventional Rolling

The UTS variation of pure Cu and Cu-Ag alloys in relation to the draw ratio is shown in Figure 15.^[1,7,55] It is found that the flow stress of pure Cu nearly saturates when the draw ratio is about 4, which is similar to those

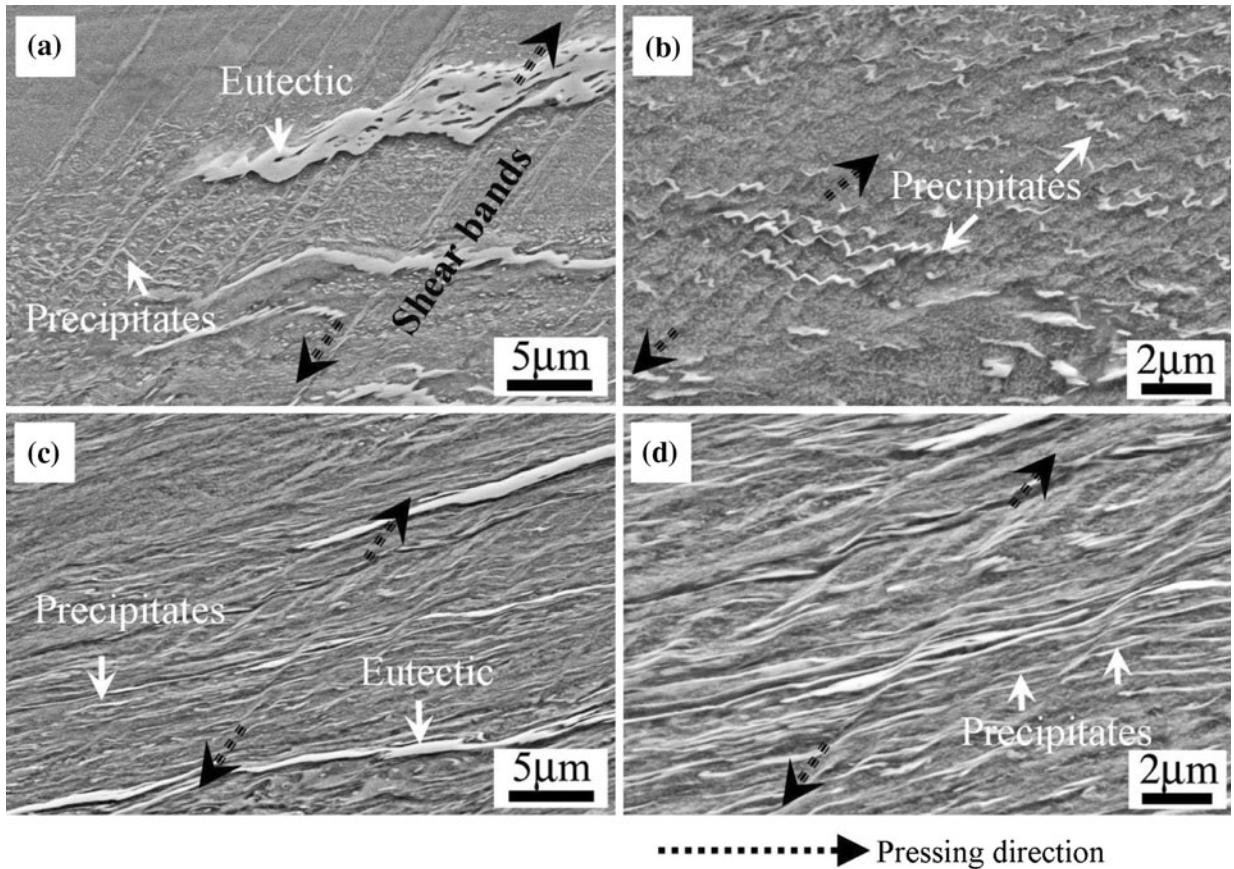


Fig. 14—Shear banding observations on specimens (a) A1, (b) A2, and (c) and (d) A4.

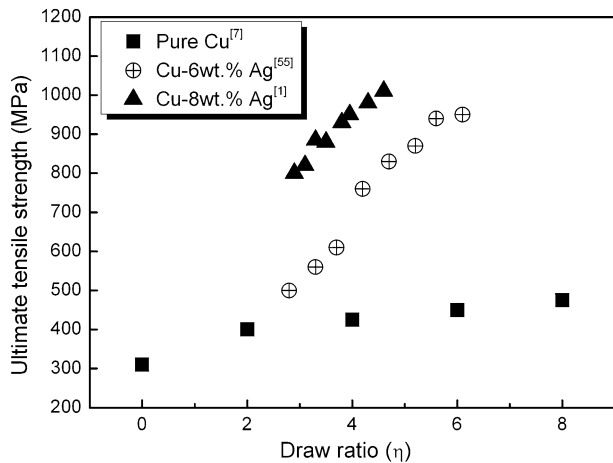


Fig. 15—UTS variations of Cu-Ag alloys^[1,55] and pure Cu^[7] in relation to the drawn ratio.

processed by ECAP.^[17] In contrast, the UTS of Cu-Ag alloys increases continuously with the draw ratio without any indication of saturation. Moreover, the UTS of Cu-Ag alloys is much higher than that of pure Cu when the draw ratio is high, indicating the existence of a high strengthening ability. It is of value to note that, for a duplex-phase Cu-Ag binary alloy processed by cold rolling or cold drawing to large strains, an *in situ*

composite with a fibrous structure and high strength approaching 2 GPa has been obtained.^[7]

For pure Cu, the variation of UTS is attributed to the strengthening effect resulting from dislocation retention and grain size refinement. In contrast, the strengthening mechanism of the Cu-Ag alloy is different because of the introduction of the eutectic component. Many researchers have paid much attention to the strengthening mechanism of such *in situ* composites.^[2-5,7,8,40,41] Generally, the modified rule of mixture is developed for the Cu-Ag alloy; for example, by estimating the strength of the regions containing dendritic Cu-rich α phase, fine silver filaments (rsf), and silver lamellae (sla), Hong and Hill^[40] have predicted the strength of the Cu-Ag alloy with the following equation:

$$\sigma_{\text{Cu-Ag}} = f_{\alpha}\sigma_{\alpha} + f_{\text{sla}}\sigma_{\text{sla}} + f_{\text{rsf}}\sigma_{\text{rsf}} \quad [2]$$

where $\sigma_{\text{Cu-Ag}}$ is the strength of the Cu-Ag composite wire, f is the volume fraction, and σ is the strength of the specified phases.

Based on the Hall-Petch relationship of the eutectic Cu-Ag alloy,^[2] the strength of the fine silver filaments can be described by the following equation^[40]:

$$\sigma_{\text{rsf}} = \sigma_0 + k\lambda^{-1/2} \quad [3]$$

where σ_0 is the intrinsic friction stress, k is the Hall-Petch coefficient, and λ is the spacing between

the Cu or Ag phase in the eutectic component. Thus, the strength of the dendritic Cu-rich α phase can be described as follows^[40]:

$$\sigma_{\alpha} = \sigma_{\text{all}} + \sigma_{\rho} + \sigma_{\text{gb}} \quad [4]$$

where σ_{all} , σ_{ρ} , and σ_{gb} are the strengthening components caused by alloying, dislocation, and grain size refinement, respectively. Then, the strength of the silver lamella can be described as follows^[7,40]:

$$\sigma_{\text{sla}} = \sigma_{\text{all}} + \alpha m \mu b / t_{\text{lamella}} \quad [5]$$

where σ_{all} is the strength of the Ag lamella caused by alloying, α is a numerical factor, m is the Taylor factor, μ is the shear modulus, b is the Burgers vector of Ag, and t_{lamella} is the average thickness of silver lamella. Their predicted results are well in agreement with the tensile strength of the as-drawn materials in their study. The model displayed reveals that the superior strength is correlated to the refined microstructure and the decreased interphase spacing in the Cu-Ag alloys. That is to say, if we can reduce the component spacing and dimensional size, then promising mechanical properties can be ameliorated.

2. Different ECAP routes

In contrast to cold rolling or drawing, the ECAP technique may be more attractive because high strain can be imposed by repeated impressing without changing the cross-section area of the sample. In addition, excellent agreement among results of ECAP, cold rolled, and cold drawn Cu-Nb duplex-phase alloys has been obtained.^[18,56] As a result, ECAP + drawing may be a better choice than drawing only.^[25] For the specimens processed by different ECAP routes up to four passes, the three-dimensional microstructures are shown in Figure 8. The eutectic component evolves into a fibrous microstructure for specimens A4 and B_A4, whereas for specimens B_C4 and C4, the eutectic component retains the coarse morphology. Considering the great discrepancies in mechanical properties and microstructures, it is suggested that the strengthening mechanism should be different for the four processing routes.

For specimens A4 and B_A4, the fibrous microstructures are similar to that processed by cold rolling or cold drawing, as shown in Figure 10. Besides the eutectic, the precipitates also are elongated severely (Figures 14(c) and (d)). In addition, the eutectic spacing decreases continuously to a relatively low level, as shown in Figure 9. Therefore, their strengthening mechanisms are supposed to be consistent with those in the cold-drawn or the cold-rolled processes. That is, besides the strengthening effect from the preeutectic component, the eutectic component also contributes significantly to the high strength, as deduced from Eqs. [3] and [5] because the dimensional sizes of λ and t_{lamella} decrease continuously, as indicated in Figure 8 (the Y plane). Note that the tensile strength of specimen A4 is higher than that of specimen B_A4, which is understandable because the deformation is concentrated in the same plane and the elongation of the eutectic is more severe for route A.

For specimens B_C4 and C4, their microstructures are greatly different from those of specimens A4 and B_A4. The eutectic component still remains relatively coarse, as shown in Figure 10. Moreover, it is shown the eutectic spacing retains a high level (Figure 9). Concerning the variation of the tensile strength as a function of passes by route B_C, the strength reaches saturation after only three passes and even decreases a little after four passes, as shown in Figure 4(a). In terms of the superior tensile strengths of the as-rolled or as-drawn Cu-Ag alloys,^[1,6,7] it is obvious that the strengthening ability of the Cu-8 wt pct Ag alloy by route B_C is restrained greatly. In contrast, the resulting tensile strength of specimen C4 is comparable with that of specimen B_C4, and both of them keep a low level. According to Eqs. [3] and [5], the dimensional sizes of λ and t_{lamella} are stable. As a result, the eutectic component shows less contribution to the strengthening effect of the Cu-Ag alloy than that during conventional drawing. Inversely, the main strengthening effect should result from the strengthening component caused by alloying, the strengthening component caused by dislocation retention, and the strengthening component caused by grain size reduction. As a result, the UTS of the Cu-Ag alloy nearly is saturated after four passes, which is similar to that of pure Cu, as shown in Figure 6. For pure Cu, the strengthening mechanism is attributed mainly to dislocation and grain size reduction.

For route A, the tensile strength increases linearly with the number of passes. According to the strengthening mechanism, the strength should increase further by increasing the passes; for route B_A, the increasing rate should be lower than that of route A, whereas for route B_C and route C, it is proposed that the strength will not increase much even after more passes.

V. CONCLUSIONS

In this work, we have conducted the Cu-8 wt pct Ag alloy in a 90 deg die with four kinds of ECAP routes (A, B_A, B_C, and C) and systematically investigated the effects of ECAP routes on the microstructural evolution and mechanical properties. The results are summarized as follows:

1. The microstructure and mechanical properties are sensitive to ECAP routes. EBSD results show that an UFG Cu-Ag alloy can be obtained most rapidly by route A; for the specimen processed by route B_C, the microstructure is rather inhomogeneous, and the mechanical properties are relatively low after four passes.
2. The specimen A4 contains the highest fraction of HABs and the finest grain structure, which are suggested to originate from the grain subdivision processes, geometrical changes of the grain shape, and the intense shear banding effect.
3. In terms of the fibrous structure and the elongated precipitates, it is proposed that eutectic components contribute to the additional effect on the higher

strength of specimens A4 and B_A4, whereas eutectic components contribute little to the strengthening of specimens B_C4 and C4.

ACKNOWLEDGMENTS

The authors are grateful for the impressive discussions with Professors T.G. Langdon, M.A. Meyers, and H. Mughrabi during their visit in IMR. Mr. L.F. Cheng, P. Zhang, X.H. An, and Ms. W. Gao also are acknowledged for their help with casting the Cu-Ag alloy, conducting the ECAP experiments, and SEM observations. This work is supported financially by National Natural Science Foundation of China (NSFC) under Grant 50890173 and 50931005 and the National Outstanding Young Scientist Foundation under Grant 50625103.

REFERENCES

1. Y. Sakai and H.-J. Schneider-Muntau: *Acta Mater.*, 1997, vol. 45, pp. 1017–23.
2. G. Frommeyer and G. Wassermann: *Acta Metall.*, 1975, vol. 23, pp. 1353–60.
3. W.A. Spitzig, A.R. Pelton, and F.C. Laabs: *Acta Metall.*, 1987, vol. 35, pp. 2427–42.
4. K. Adachi, S. Tsubokawa, T. Takeuchi, and H.G. Suzuki: *J. Jpn. Inst. Met.*, 1997, vol. 61, pp. 397–403.
5. P.D. Funkenbusch and T.H. Courtney: *Scripta Metall.*, 1981, vol. 15, pp. 1349–54.
6. Y. Sakai, K. Inoue, T. Asano, H. Wada, and H. Maeda: *Appl. Phys. Lett.*, 1991, vol. 59, pp. 2965–67.
7. A. Benghalem and D.G. Morris: *Acta Mater.*, 1997, vol. 45, pp. 397–406.
8. J.D. Embury and R.M. Fisher: *Acta Metall.*, 1966, vol. 14, pp. 147–59.
9. R.Z. Valiev, R.K. Islamgaliev, and I.V. Alexandrov: *Prog. Mater. Sci.*, 2000, vol. 45, pp. 103–89.
10. Y.T. Zhu, T.C. Lowe, and T.G. Langdon: *Scripta Mater.*, 2004, vol. 51, pp. 825–30.
11. S.C. Wang, M.J. Starink, N. Gao, X.G. Qiao, C. Xu, and T.G. Langdon: *Acta Mater.*, 2008, vol. 56, pp. 3800–09.
12. P.L. Sun, P.W. Kao, and C.P. Chang: *Metall. Mater. Trans. A*, 2004, vol. 35A, pp. 1359–68.
13. Y.T. Zhu, J.Y. Huang, J. Gubicza, T. Ungar, Y.M. Wang, E. Ma, and R.Z. Valiev: *J. Mater. Res.*, 2003, vol. 18, pp. 1908–17.
14. Y.H. Zhao, X.Z. Liao, Z. Jin, R.Z. Valiev, and Y.T. Zhu: *Acta Mater.*, 2004, vol. 52, pp. 4589–99.
15. T.G. Langdon, M. Furukawa, M. Nemoto, and Z. Horita: *JOM*, 2000, vol. 52, pp. 30–33.
16. A. Mishra, B.K. Kad, F. Gregori, and M.A. Meyers: *Acta Mater.*, 2007, vol. 55, pp. 13–28.
17. F. Dalla Torre, R. Lapovok, J. Sandlin, P.F. Thomson, C.H.J. Davies, and E.V. Pereloma: *Acta Mater.*, 2004, vol. 52, pp. 4819–32.
18. V.M. Segal, K.T. Hartwig, and R.E. Goforth: *Mater. Sci. Eng. A*, 1997, vol. 224A, pp. 107–15.
19. A.P. Zhilyaev and T.G. Langdon: *Prog. Mater. Sci.*, 2008, vol. 53, pp. 893–979.
20. Y.S. Li, N.R. Tao, and K. Lu: *Acta Mater.*, 2008, vol. 56, pp. 230–41.
21. N.R. Tao and K. Lu: *J. Mater. Sci. Technol.*, 2007, vol. 23, pp. 771–74.
22. Y. Saito, H. Utsunomiya, N. Tsuji, and T. Sakai: *Acta Mater.*, 1999, vol. 47, pp. 579–83.
23. M. Furukawa, Y. Iwahashi, Z. Horita, M. Nemoto, and T.G. Langdon: *Mater. Sci. Eng. A*, 1998, vol. 257, pp. 328–32.
24. L.R. Cornwell, K.T. Hartwig, R.E. Goforth, and S.L. Semiatin: *Mater. Charact.*, 1996, vol. 37, pp. 295–300.
25. T.S. Edgcombe Summers, V.M. Segal, K.T. Hartwig, R.E. Goforth, R.P. Walsh, and P. Pernambuco-Wise: *Adv. Cryogen Eng.*, 1996, vol. 42, pp. 499–505.
26. Y.T. Zhu and T.C. Lowe: *Mater. Sci. Eng. A*, 2000, vol. 291, pp. 46–53.
27. K. Oh-Ishi, Z. Horita, M. Furukawa, M. Nemoto, and T.G. Langdon: *Metall. Mater. Trans. A*, 1998, vol. 29A, pp. 2011–13.
28. V.V. Stolyarov, Y.T. Zhu, I.V. Alexandrov, T.C. Lowe, and R.Z. Valiev: *Mater. Sci. Eng. A*, 2001, vol. 299, pp. 59–67.
29. P.B. Prangnell, A. Gholinia, and M.V. Markushev: in *Investigations and Applications of Severe Plastic Deformation*, T.C. Lowe and R.Z. Valiev, eds., Kluwer Academic Publishers, Dordrecht, The Netherlands, 2000, pp. 65–71.
30. A. Gholinia, P.B. Prangnell, and M.V. Markushev: *Acta Mater.*, 2000, vol. 48, pp. 1115–30.
31. Y. Iwahashi, Z. Horita, M. Nemoto, and T.G. Langdon: *Acta Mater.*, 1997, vol. 45, pp. 4733–41.
32. Y. Iwahashi, Z. Horita, M. Nemoto, and T.G. Langdon: *Acta Mater.*, 1998, vol. 46, pp. 3317–31.
33. S. Li: *Scripta Mater.*, 2009, vol. 60, pp. 706–09.
34. I.J. Beyerlein, R.A. Lebensohn, and C.N. Tomé: *Mater. Sci. Eng. A*, 2003, vol. 345, pp. 122–38.
35. Y. Iwahashi, J. Wang, Z. Horita, M. Nemoto, and T.G. Langdon: *Scripta Mater.*, 1996, vol. 35, pp. 143–46.
36. Y. Iwahashi, M. Furukawa, Z. Horita, M. Nemoto, and T.G. Langdon: *Metall. Mater. Trans. A*, 1998, vol. 29A, pp. 2245–52.
37. Y.Z. Tian and Z.F. Zhang: *Mater. Sci. Eng. A*, 2009, vol. 508, pp. 209–13.
38. S. Nagasaki and M. Hirabayashi: *Binary Alloy Phase-Diagrams*, AGNE Gijyutsu Center, Co., Ltd, Tokyo, Japan, 2002.
39. J. Lin and L. Meng: *J. Alloy. Compd.*, 2008, vol. 454, pp. 150–55.
40. S.I. Hong and M.A. Hill: *Acta Mater.*, 1998, vol. 46, pp. 4111–22.
41. K. Han, A.A. Vasquez, Y. Xin, and P.N. Kalu: *Acta Mater.*, 2003, vol. 51, pp. 767–80.
42. Y.Z. Tian, Z.F. Zhang, and Z.G. Wang: *Phil. Mag.*, 2009, vol. 89, pp. 1715–30.
43. S. Qu, X.H. An, H.J. Yang, C.X. Huang, G. Yang, Q.S. Zang, Z.G. Wang, S.D. Wu, and Z.F. Zhang: *Acta Mater.*, 2009, vol. 57, pp. 1586–601.
44. R.Z. Valiev, I.V. Alexandrov, Y.T. Zhu, and T.C. Lowe: *J. Mater. Res.*, 2002, vol. 17, pp. 5–8.
45. Y.H. Zhao, J.F. Bingert, X.Z. Liao, B.Z. Cui, K. Han, A.V. Sergueeva, A.K. Mukherjee, R.Z. Valiev, T.G. Langdon, and Y.T. Zhu: *Adv. Mater.*, 2006, vol. 18, pp. 2949–53.
46. L. Lu, Y. Shen, X. Chen, L. Qian, and K. Lu: *Science*, 2004, vol. 304, pp. 422–26.
47. M.E. Launey and R.O. Ritchie: *Adv. Mater.*, 2009, vol. 21, pp. 1–8.
48. W.D. Callister, Jr.: *Fundamentals of Materials Science and Engineering*, 5th ed., John Wiley & Sons Inc., New York, NY, 2001.
49. P.J. Apps, J.R. Bowen, and P.B. Prangnell: *Acta Mater.*, 2003, vol. 51, pp. 2811–22.
50. M. Furukawa, Z. Horita, and T.G. Langdon: *Mater. Sci. Eng. A*, 2002, vol. 332A, pp. 97–109.
51. P.B. Prangnell, J.R. Bowen, and P.J. Apps: *Mater. Sci. Eng. A*, 2004, vol. 375-7A, pp. 178–85.
52. O.V. Mishin and A. Godfrey: *Metall. Mater. Trans. A*, 2008, vol. 39A, pp. 2923–30.
53. M. Berta, P.J. Apps, and P.B. Prangnell: *Mater. Sci. Eng. A*, 2005, vol. 410-1A, pp. 381–85.
54. Y.Z. Tian, W.Z. Han, H.J. Yang, S.X. Li, S.D. Wu, and Z.F. Zhang: *Scripta Mater.*, 2010, vol. 62, pp. 183–86.
55. J.B. Liu, L. Meng, and Y.W. Zeng: *Mater. Sci. Eng. A*, 2006, vols. 435–436, pp. 237–44.
56. C.L. Trybus and W.A. Spitzig: *Acta Metall.*, 1989, vol. 37, pp. 1971–81.